Computer Assisted Mechanics and Engineering Sciences, 7: 53–67, 2000.

Finite element analysis for multi-leaf structures with frictional contact and large deformation

Xian Chen, Kazuhiro Nakamura, Masahiko Mori
Takasago R&D Center, Mitsubishi Heavy Industries, Ltd.
2-1-1, Shinhama Arai-Cho, Takasago, Hyogo Pref. 676-8686, Japan

Toshiaki Hisada
Department of Mechano-Informatics, The University of Tokyo
7-3-1 Hongo, Bunkyo-Ku, Tokyo, 113-0033, Japan

(Received March 8, 1999)

The analysis of multi-leaf structures should be performed taking friction into account. The objectivity of friction law should be preserved because large deformation generally occurs. By use of the convected coordinate system, the objectivity can be preserved naturally. Therefore, in finite element analysis, the element local coordinate system can be used. However, when a contact point slides over the element boundary, a problem arises due to the discontinuity of the local coordinates between elements. In this work, an algorithm is proposed, i.e., the formulation is essentially based on the convected coordinate system while the sliding term is redefined as a spatial vector and is calculated in the reference configuration. Thus, the finite sliding due to large deformation can be treated without paying special attention to the limit of the local coordinate system. Two numerical examples including a simplified model of a leaf spring structure used in nuclear power plants are given.

1. Introduction

Multi-leaf structures are widely used in automobiles and many other engineering fields. In such structures, the frictional contact phenomenon is an important factor which affects the structural response. Since large deformation generally occurs, finite sliding on the contact surface should be taken into account in the analysis.

Although the frictional contact problem can be mathematically characterized with variational inequality [4], the analytical solution can only be obtained for special cases. The development of the finite element method provides an actual means to analyze frictional contact problems [4, 10, 11]. The geometrical constraint on the contact surface can be treated by introducing the Lagrange multiplier method or penalty method [4, 10], or other modified Lagrangian approaches such as the augmented Lagrangian method (e.g. [8]) and perturbed Lagrangian method (e.g. [9]). On the other hand, to overcome the obstacle of nondifferentiability of the classic Coulomb's law, friction laws, which are analogous to the elastoplastic constitutive law, have been adopted recently [2, 7]. In addition the orthotropic frictional contact problems were investigated by the use of two friction functions in the orthogonal directions to account for the orthotropic properties of friction [2].

In frictional contact problems with large deformation, the objectivity of the friction law should be preserved. For this purpose, the objective rate of tangential and normal traction on the contact surface was introduced [4]. On the other hand, a finite element analysis approach based on the convected coordinate system was proposed for large deformation frictional contact problems [5]. This approach seems reasonable because the relative velocity of contact points is well described by the convected coordinates, i.e., the objectivity of the friction law can be preserved without introducing the objective rate. However, since it is difficult to define a general convected coordinate

system for the whole contact surface, the element local coordinate system is used as a substitute. From this point of view, it is not easy, using the approach presented by Laursen *et al.* [5], to deal with the sliding that occurs over the element boundary where local coordinates are discontinuous. To overcome this problem, Parisch *et al.* [6] used a global coordinate system but the objectivity of the friction law was not discussed.

In this paper, for the treatment of the frictional contact problem in multi-leaf structures, we propose a method for solving the above problem. In this method, the formulation is essentially based on a convected coordinate system, while the sliding term is redefined as a spatial vector and is calculated using the reference configuration. The finite sliding can thus be treated, regardless of the limitations of element coordinate systems. Furthermore, the corresponding consistent tangent stiffness due to frictional contact is derived to assure quadratic convergence. The effectiveness of the proposed method is verified by two numerical examples including a simplified model of a leaf spring structure used in nuclear power plants. The effect of friction on the structural response is revealed to cause another path dependence besides the elastoplastic one.

2. Finite element formulation for frictional contact problems

2.1. Basic relations

Assume that two bodies, 1 and 2, contact each other on the surface ${}^t\gamma_c^1$ of body 1 and ${}^t\gamma_c^2$ of body 2 at time t. Denoting the virtual displacements as $\delta\boldsymbol{u}^1$ and $\delta\boldsymbol{u}^2$, the virtual work done by the contact forces ${}^t\boldsymbol{p}^1$ and ${}^t\boldsymbol{p}^2$ is given as follows,

$$\begin{aligned}\delta {}^tW_c &= \int_{{}^t\gamma_c^1} {}^t\boldsymbol{p}^1 \cdot \delta\boldsymbol{u}^1 \,\mathrm{d}s + \int_{{}^t\gamma_c^2} {}^t\boldsymbol{p}^2 \cdot \delta\boldsymbol{u}^2 \,\mathrm{d}s \\ &= \int_{{}^t\gamma_c} \left[{}^tp_n \, {}^t\boldsymbol{n} \cdot (\delta\boldsymbol{u}^1 - \delta\boldsymbol{u}^2) + {}^tp_t \, {}^t\boldsymbol{t} \cdot (\delta\boldsymbol{u}^1 - \delta\boldsymbol{u}^2) \right] \mathrm{d}s, \end{aligned} \tag{1}$$

where ${}^t\boldsymbol{n}^i$ and ${}^t\boldsymbol{t}^i$ are the outer normal vector and the tangential vector on the contact surface of body i. Also, the following relations are used in writing the above equation,

$$ {}^t\gamma_c \equiv {}^t\gamma_c^1 = {}^t\gamma_c^2, \tag{2}$$

$$ {}^t\boldsymbol{p}^1 = {}^tp_n^1 \, {}^t\boldsymbol{n}^1 + {}^tp_t^1 \, {}^t\boldsymbol{t}^1, \qquad {}^t\boldsymbol{p}^2 = {}^tp_n^2 \, {}^t\boldsymbol{n}^2 + {}^tp_t^2 \, {}^t\boldsymbol{t}^2, \tag{3}$$

$$ {}^t\boldsymbol{n} \equiv {}^t\boldsymbol{n}^1 = -{}^t\boldsymbol{n}^2, \qquad {}^t\boldsymbol{t} \equiv {}^t\boldsymbol{t}^1 = -{}^t\boldsymbol{t}^2, \tag{4}$$

$$ {}^tp_n \equiv {}^tp_n^1 = {}^tp_n^2, \qquad {}^tp_t \equiv {}^tp_t^1 = {}^tp_t^2. \tag{5}$$

Next, defining the penetration with the contact points ${}^t\boldsymbol{x}^1$ and ${}^t\boldsymbol{x}^2$ of each body, as

$$ {}^tg = ({}^t\boldsymbol{x}^2 - {}^t\boldsymbol{x}^1) \cdot {}^t\boldsymbol{n}, \tag{6}$$

the mechanical and geometrical constraint conditions are given by the following equations,

$$ {}^tp_n \le 0, \qquad {}^tg \ge 0, \qquad {}^tp_n \cdot {}^tg = 0. \tag{7}$$

Thus, the virtual work equation and the constraint condition are written in the weak form using the reference configuration:

$$\delta {}^tW_c = \int_{\Gamma_c} \left[{}^t\tilde{p}_n \, {}^t\boldsymbol{n} \cdot (\delta\boldsymbol{u}^1 - \delta\boldsymbol{u}^2) + {}^t\tilde{p}_t \, {}^t\boldsymbol{t} \cdot (\delta\boldsymbol{u}^1 - \delta\boldsymbol{u}^2) \right] \mathrm{d}S, \tag{8}$$

$$\int_{\Gamma_c} \delta \, {}^t\tilde{p}_n \cdot {}^tg \,\mathrm{d}S = 0, \tag{9}$$

where Γ_c denotes the contact area before deformation, ${}^t\tilde{p}_n \, {}^t\boldsymbol{n}$ and ${}^t\tilde{p}_t \, {}^t\boldsymbol{t}$ are the normal and tangential part of the nominal contact force vector, and ${}^t\tilde{p}_n$ corresponds to the Lagrange multiplier.

Although ˜ represents the nominal value in the above equation, it will be omitted for the sake of brevity in the following sections. Likewise, the normal and tangential components of the contact force will simply be called contact force and friction force, respectively.

2.2. Virtual work equation in convected coordinate system

Objective friction law is derived using a convected coordinate system [5]. In this section, contact and friction forces are represented in a convected coordinate system, by which the virtual work equation is expressed. Figure 1 shows the surfaces of bodies 1 and 2. The hitting point $\boldsymbol{x}^h$ of body 2 is going to contact the target point $\boldsymbol{x}^t$ of body 1, where $\boldsymbol{x}^t$ is determined by drawing a line perpendicular to the surface of body 2 from $\boldsymbol{x}^h$. The left superscript t, denoting time, is omitted hereafter, and

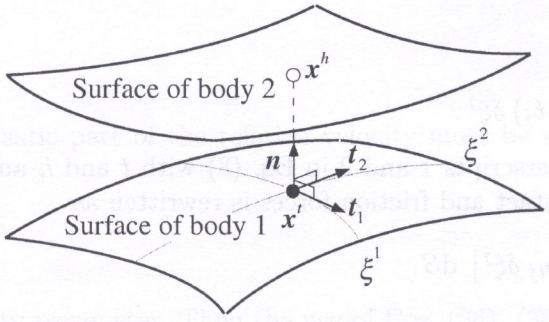

Fig. 1. Contact surfaces

the right superscripts h and t represent the hitting and target points, respectively. In Fig. 1, ξ^1 and ξ^2 indicate the convected coordinates at $\boldsymbol{x}^t$, $\boldsymbol{t}_1$ and $\boldsymbol{t}_2$ indicate the covariant base vectors, and $\boldsymbol{n}$ indicates the outer normal vector with unit length. Namely,

$$\boldsymbol{t}_1 = \frac{\partial \boldsymbol{x}^t}{\partial \xi^1}, \qquad \boldsymbol{t}_2 = \frac{\partial \boldsymbol{x}^t}{\partial \xi^2}, \tag{10}$$

$$\boldsymbol{r} \equiv \boldsymbol{t}_1 \times \boldsymbol{t}_2, \qquad \boldsymbol{n} = \frac{\boldsymbol{r}}{|\boldsymbol{r}|}. \tag{11}$$

It should be noted, from the definition of the target point, that the kinematic movement of $\boldsymbol{x}^t$ depends not only on the deformation of body 1 but also on the motion of $\boldsymbol{x}^h$, i.e., the slip of $\boldsymbol{x}^h$ relative to the surface of body 1. Thus, using the convected coordinate system and summation convention, the differentiation of $\boldsymbol{x}^t$ can be given as

$$\mathrm{d}\boldsymbol{x}^t(\xi^1, \xi^2, t) = \mathrm{d}\boldsymbol{u}^t + \boldsymbol{t}_i \, \mathrm{d}\xi^i . \tag{12}$$

For the material point of body 1, with a convected coordinate where $\boldsymbol{x}^t$ has been determined, $d\boldsymbol{u}^t$ represents the infinitesimal displacement (material time derivative) of this point due to the deformation of body 1. Also, $\boldsymbol{t}_i d\xi^i$ indicates the movement (slip) relative to body 2. The introduction of vector

$$\boldsymbol{g} \equiv (\boldsymbol{x}^t - \boldsymbol{x}^h) \tag{13}$$

and the use of the definitions of penetration and contact point (Fig. 1) yield

$$g \equiv \boldsymbol{g} \cdot \boldsymbol{n}, \tag{14}$$

$$\boldsymbol{g} = g\,\boldsymbol{n} \tag{15}$$

$$\boldsymbol{t}_i \cdot \boldsymbol{g} = 0, \qquad (i = 1, 2). \tag{16}$$

The variation of $\boldsymbol{g}$ is obtained as

$$\delta \boldsymbol{g} = \boldsymbol{t}_i \, \delta\xi^i + \delta \boldsymbol{u}^t - \delta \boldsymbol{u}^h \tag{17}$$

by considering the dependence of $\boldsymbol{x}^t$ on $\boldsymbol{x}^h$. Since the base vector of the convected coordinate system is perpendicular to the normal vector, it follows that

$$\boldsymbol{n} \cdot (\delta \boldsymbol{u}^t - \delta \boldsymbol{u}^h) = \boldsymbol{n} \cdot \delta \boldsymbol{g} \, . \tag{18}$$

Also, from Eqs. (13) and (17), the variation of Eq. (16) is given by

$$\delta \boldsymbol{t}_i \cdot (\boldsymbol{x}^t - \boldsymbol{x}^h) + (\boldsymbol{t}_i \cdot \boldsymbol{t}_j) \, \delta\xi^j + \boldsymbol{t}_i \cdot (\delta \boldsymbol{u}^t - \delta \boldsymbol{u}^h) = 0 \, . \tag{19}$$

Since in the equilibrium state,

$$\boldsymbol{g} = (\boldsymbol{x}^t - \boldsymbol{x}^h) = \boldsymbol{0} \tag{20}$$

must be satisfied, we have

$$\boldsymbol{t}_i \cdot (\delta \boldsymbol{u}^t - \delta \boldsymbol{u}^h) = -(\boldsymbol{t}_i \cdot \boldsymbol{t}_j) \, \delta\xi^j \, . \tag{21}$$

Thus, by replacing the superscripts 1 and 2 in Eq. (8) with t and h and using Eqs. (18) and (21), the virtual work due to contact and friction forces is rewritten as

$$\delta W_c = \int_{\Gamma_c} \left[p_n \, \boldsymbol{n} \cdot \delta \boldsymbol{g} - p_{tj} \, \delta\xi^j \right] \mathrm{d}S \tag{22}$$

where p_{tj} is the covariant component of the friction force vector $\boldsymbol{p}_t$ which is decomposed with the covariant base vector as

$$\boldsymbol{p}_t \equiv p_t \, \boldsymbol{t} = p_t^i \, \boldsymbol{t}_i \, . \tag{23}$$

Additionally, the relationship between the covariant and contravariant components is used, namely,

$$p_{tj} = (\boldsymbol{t}_i \cdot \boldsymbol{t}_j) p_t^i \, . \tag{24}$$

2.3. Friction law

To avoid the discontinuity of mechanical response, friction laws similar to the constitutive relationship of elastoplasticity have been proposed [2, 7], i.e., small slip is allowed, even in the stick state. Such procedures essentially introduce a penalty constraint for sticking. For the material points of bodies 1 and 2, located at $\boldsymbol{x}^t$ and $\boldsymbol{x}^h$, the difference between their material time derivatives gives the relative displacement velocity, which can then be expressed with the normal component $\dot{\boldsymbol{u}}_n$ and tangential component $\dot{\boldsymbol{u}}_t$ as

$$\dot{\boldsymbol{u}} = \dot{\boldsymbol{u}}^t - \dot{\boldsymbol{u}}^h = \dot{\boldsymbol{u}}_n + \dot{\boldsymbol{u}}_t \, . \tag{25}$$

Moreover, the use of the additive decomposition of the tangential component into the elastic part (stick) and plastic part (slip) leads to

$$\dot{\boldsymbol{u}}_t = \dot{\boldsymbol{u}}_t^e + \dot{\boldsymbol{u}}_t^p \, . \tag{26}$$

On the other hand, in the equilibrium state, the normal component becomes

$$\dot{\boldsymbol{u}}_n = \dot{\boldsymbol{u}}_n^e = \dot{\boldsymbol{u}}_n^p = \boldsymbol{0} \tag{27}$$

due to the geometrical constraint condition. The slip condition which corresponds to the yield condition takes the form

$$\phi = |\boldsymbol{p}_t| - \mu |\boldsymbol{p}_n| = 0 \tag{28}$$

where μ, $\boldsymbol{p}_t$ and $\boldsymbol{p}_n$ are the friction coefficient, friction force and contact force, respectively. Although the yield function is taken as the plastic potential in the flow rule of elastoplasticity theory, the frictional potential is defined for frictional problems as

$$\Psi = |\boldsymbol{p}_t| \tag{29}$$

when Eq. (27) is considered. Thus, the flow rule may be written as follows:

$$\dot{\boldsymbol{u}}_t^p = -\dot{\lambda}\,\frac{\partial \Psi}{\partial \boldsymbol{p}_t} = -\dot{\lambda}\,\frac{\boldsymbol{p}_t}{|\boldsymbol{p}_t|}\,, \tag{30}$$

$$\dot{\lambda} \geq 0\,. \tag{31}$$

Next, let the velocity of friction force be decomposed with the contravariant base vectors of the convected coordinate as

$$\dot{\boldsymbol{p}}_t = \dot{p}_{ti}\,\boldsymbol{t}^i\,. \tag{32}$$

Due to the fact that the elastic part of the relative velocity must be small enough, the following form can be obtained:

$$\dot{\boldsymbol{u}}_t^e = -\frac{\dot{\boldsymbol{p}}_t}{\varepsilon} = -\frac{\dot{p}_{ti}\,\boldsymbol{t}^i}{\varepsilon} \tag{33}$$

where ε indicates the penalty parameter. Then the use of Eqs. (26), (30) and (33) leads to

$$-\frac{\dot{p}_{ti}\,\boldsymbol{t}^i}{\varepsilon} = \dot{\boldsymbol{u}}_t + \dot{\lambda}\,\frac{\boldsymbol{p}_t}{|\boldsymbol{p}_t|}\,. \tag{34}$$

Referring to Eq. (17), in the equilibrium state, the time derivative of Eq. (20) becomes

$$\boldsymbol{t}_i\dot{\xi}^i + \dot{\boldsymbol{u}}^t - \dot{\boldsymbol{u}}^h = \boldsymbol{0}\,. \tag{35}$$

From this equation, as well as Eqs. (25) and (27) and the relationship between the covariant and contravariant base vectors, namely,

$$\boldsymbol{t}_i = (\boldsymbol{t}_i \cdot \boldsymbol{t}_j)\,\boldsymbol{t}^j\,, \tag{36}$$

it can be obtained that

$$\dot{\boldsymbol{u}}_t = -\boldsymbol{t}_i\dot{\xi}^i = -(\boldsymbol{t}_i \cdot \boldsymbol{t}_j)\,\dot{\xi}^i\boldsymbol{t}^j\,. \tag{37}$$

Finally, by substituting this equation into Eq. (34) and combining the result with Eqs. (30) and (31), the friction law is derived as follows:

$$\phi \quad = |\boldsymbol{p}_t| - \mu|\boldsymbol{p}_n| \leq 0\,, \tag{38a}$$

$$\dot{p}_{ti}\boldsymbol{t}^i = \varepsilon\left[(\boldsymbol{t}_i \cdot \boldsymbol{t}_j)\dot{\xi}^j - \dot{\lambda}\,\frac{p_{ti}}{|\boldsymbol{p}_t|}\right]\boldsymbol{t}^i\,, \tag{38b}$$

$$\dot{\lambda} \quad \geq 0\,, \tag{38c}$$

$$\phi \cdot \dot{\lambda} = 0\,. \tag{38d}$$

Furthermore, the left-hand side of Eq. (38b) and the first term on the right-hand side are in the form of the Oldroyd rate of a vector. As well, the second term on the right-hand side includes a scalar and a product of the friction force vector with its norm. Thus, it is clear that the friction equations satisfy the objectivity requirement.

3. Analysis of frictional contact problems with large sliding

3.1. Incremental decomposition of friction law

Due to the deformation path dependence of frictional problems, it is necessary to carry out an incremental analysis. Using the formulas of Sec. 1, it is, in principle, possible to compute the increments of friction force and sliding by the incremental decomposition. Using the backward Euler integration for incremental analysis, the incremental form of Eq. (38) becomes

$$\phi_{(i+1)} = |\boldsymbol{p}_{t(i+1)}| - \mu|\boldsymbol{p}_{n(n+1)}| \leq 0\,, \tag{39a}$$

$$p_{tk(i+1)}\,\boldsymbol{t}^k_{(i+1)} = p_{tk(i)}\,\boldsymbol{t}^k_{(i+1)} + \varepsilon\left[(\boldsymbol{t}_k \cdot \boldsymbol{t}_j)_{(i+1)}\left(\xi^j_{(i+1)} - \xi^j_{(i)}\right) - \Delta\lambda\,\frac{p_{tk(i+1)}}{|\boldsymbol{p}_{t(i+1)}|}\right]\boldsymbol{t}^k_{(i+1)}\,, \tag{39b}$$

$$\Delta\lambda \geq 0\,, \tag{39c}$$

$$\phi_{(i+1)} \cdot \Delta\lambda = 0\,, \tag{39d}$$

where subscripts (i) and $(i+1)$ indicate the incremental steps. Considering Eq. (39b), the increment of the convected coordinate appears as the result of incremental decomposition. In the finite element method, the contact surface is divided into elements and the local coordinate of every element is used practically as a convected coordinate. Thus, the increment of a convected coordinate cannot be computed if the contact point slides over the boundary of element. Because of the difficulty of defining a general convected coordinate on the whole contact surface for an arbitrary body, in [5] the element local coordinate was extended as an expedient. However, since this treatment requires a control of the load increment in order to limit sliding over elements, it is considered impractical for the *a priori* unknown contact state of a deforming body.

In this work, the following approach is presented to overcome this problem. Defining

$$\Delta\boldsymbol{r} \equiv (\boldsymbol{t}_k \cdot \boldsymbol{t}_j)_{(i+1)}\left(\xi^j_{(i+1)} - \xi^j_{(i)}\right)\boldsymbol{t}^k_{(i+1)} \tag{40}$$

for the term in Eq. (39b), including the increment of the convected coordinate, it is clear from Eq. (37) that $\Delta\boldsymbol{r}$ represents the increment of relative displacement for the contact points. By referring to the discretized contact surfaces shown in Fig. 2, $\Delta\boldsymbol{r}$ can be approximated with

$$\Delta\boldsymbol{r} \doteq \boldsymbol{x}^t_{(i+1)} - \boldsymbol{x}^t_{(i)} \tag{41}$$

where $\boldsymbol{x}^t_{(i+1)}$ is the position vector of the contact point at increment $i+1$, whereas $\boldsymbol{x}^t_{(i)}$ is the position vector, at increment $i+1$, of the material point where the contact point has been located at increment i. However, because of movement due to deformation, $\boldsymbol{x}^t_{(i)}$ is unknown at increment $i+1$. Because this movement affects the tangent stiffness due to friction, it is not convenient to use Eq. (41) directly. Now a mapping of the contact point to the reference configuration, as shown in Fig. 3, is considered. Let $\boldsymbol{F}$ be the deformation gradient tensor, $\boldsymbol{t}_{j(i+1)}$ the covariant base vector at the contact point $\boldsymbol{x}^t_{(i+1)}$ in the current configuration (increment $i+1$), and ${}^0\boldsymbol{t}_{j(i+1)}$ the covariant base vector at the mapped point $\boldsymbol{X}^t_{(i+1)}$ in the reference configuration. Use of the relationship [3]

$$\boldsymbol{F} = \delta^j_k\left(\boldsymbol{t}_{j(i+1)} \otimes {}^0\boldsymbol{t}^k_{(i+1)}\right) \tag{42}$$

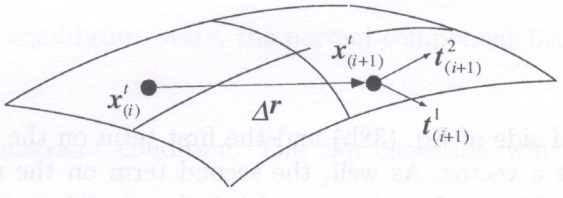

Fig. 2. Discretized contact surface

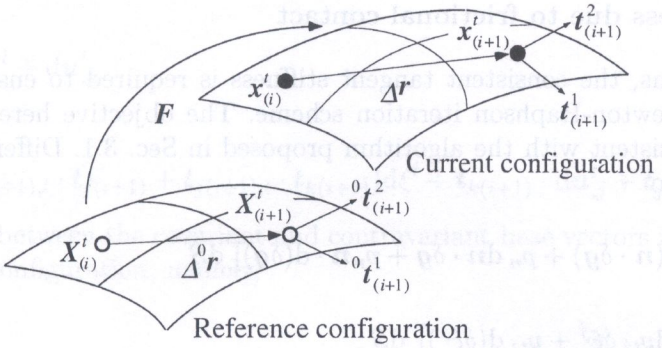

Fig. 3. Motion of contact surface

gives

$$\Delta \boldsymbol{r} = \left(\boldsymbol{t}_{j(i+1)} \cdot \boldsymbol{t}_{k(i+1)}\right) \left({}^0\boldsymbol{t}^k_{i+1} \cdot \Delta^0 \boldsymbol{r}\right) \boldsymbol{t}^j_{(i+1)} \tag{43}$$

where

$$\Delta^0 \boldsymbol{r} \equiv \left(\xi^j_{(i+1)} - \xi^j_{(i)}\right) {}^0\boldsymbol{t}_{j(i+1)} \tag{44}$$

is the relative displacement increment mapped to the reference configuration and can be calculated as

$$\Delta^0 \boldsymbol{r} \doteq \boldsymbol{X}^t_{(i+1)} - \boldsymbol{X}^t_{(i)} \tag{45}$$

Thus, because $\boldsymbol{X}^t_{(i)}$ in Eq. (45) is fixed to the reference configuration, its influence on the frictional tangent stiffness vanishes and only the change of $\boldsymbol{X}^t_{(i+1)}$ has to be considered. Finally, the use of Eqs. (40) and (43) with Eq. (39) results in

$$p_{tk(i+1)} \boldsymbol{t}^k_{(i+1)} = p_{tk(i)} \boldsymbol{t}^k_{(i+1)} + \varepsilon \left[(\boldsymbol{t}_k \cdot \boldsymbol{t}_j)_{(i+1)} \left({}^0\boldsymbol{t}^j_{(i+1)} \cdot \Delta^0 \boldsymbol{r}\right) - \Delta\lambda \frac{p_{tk(i+1)}}{|\boldsymbol{p}_{t(i+1)}|} \right] \boldsymbol{t}^k_{(i+1)} . \tag{46}$$

The mapped contact point can be obtained from its element local coordinate in the current configuration and the node coordinate before deformation.

The algorithm adopted to update friction force is analogous to the radial return approach in elastoplasticity analysis. First, assuming the stick state, the trial friction force is found from

$$p^{(T)}_{tk(i+1)} = p_{tk(i)} + \varepsilon (\boldsymbol{t}_k \cdot \boldsymbol{t}_j)_{(i+1)} \left({}^0\boldsymbol{t}^j_{(i+1)} \cdot \Delta^0 \boldsymbol{r}\right) . \tag{47}$$

If the result satisfies

$$\left|\boldsymbol{p}^{(T)}_{t(i+1)}\right| - \mu \left|\boldsymbol{p}_{n(i+1)}\right| \leq 0 \tag{48}$$

then the final friction force is determined as

$$p^{(F)}_{tk(i+1)} = p^{(T)}_{tk(i+1)} . \tag{49}$$

Otherwise, if the trial friction force results in

$$\left|\boldsymbol{p}^{(T)}_{t(i+1)}\right| - \mu \left|\boldsymbol{p}_{n(i+1)}\right| > 0 \tag{50}$$

then, in order to pull the state point back onto the yield surface, it has to be modified as follows:

$$T_{k(i+1)} \equiv \frac{p^{(T)}_{ik(i+1)}}{\left|\boldsymbol{p}^{(T)}_{t(i+1)}\right|} , \tag{51}$$

$$p^{(F)}_{tk(i+1)} = \mu \left|\boldsymbol{p}_{n(i+1)}\right| T_{k(i+1)} . \tag{52}$$

3.2. Tangent stiffness due to frictional contact

For nonlinear problems, the consistent tangent stiffness is required to ensure a quadratic rate of convergence of the Newton-Raphson iteration scheme. The objective here is to obtain a tangent stiffness which is consistent with the algorithm proposed in Sec. 3.1. Differentiation of the virtual work equation leads to

$$\begin{aligned} \mathrm{d}(\delta W_c) = & \int_{\Gamma_c} [\mathrm{d}p_n(\boldsymbol{n}\cdot\delta\boldsymbol{g}) + p_n\,\mathrm{d}\boldsymbol{n}\cdot\delta\boldsymbol{g} + p_n\boldsymbol{n}\cdot\mathrm{d}(\delta\boldsymbol{g})]\,\mathrm{d}S \\ & - \int_{\Gamma_c} \left[\mathrm{d}p_{tj}\,\delta\xi^j + p_{tj}\,\mathrm{d}(\delta\xi^j)\right]\,\mathrm{d}S \end{aligned} \tag{53}$$

where $\mathrm{d}p_n$ is treated as the dependent variable, in the case of using the Lagrange multiplier constraint. Let the differentiation of friction force be derived later. By referring to Sec. 2.2 and considering the geometrical relationship on the contact surface and the fact that $\boldsymbol{x}^t$ is affected by $\boldsymbol{x}^h$, the differentiation of the other terms can be obtained in the following way. The definition of

$$\boldsymbol{a}_{,i} \equiv \frac{\partial \boldsymbol{a}}{\partial \xi^i}\,, \tag{54}$$

$$\boldsymbol{b}_{,ij} \equiv \frac{\partial^2 \boldsymbol{b}}{\partial \xi^i \partial \xi^j}\,, \tag{55}$$

will be used hereafter.

Noting that $\delta\boldsymbol{n}\cdot\boldsymbol{n} = 0$, the variation of Eq. (15) becomes

$$p_n\,\mathrm{d}\boldsymbol{n}\cdot\delta\boldsymbol{g} = p_n g\,\mathrm{d}\boldsymbol{n}\cdot\delta\boldsymbol{n} \tag{56}$$

The differentiation of Eq. (17) leads to

$$p_n\boldsymbol{n}\cdot\mathrm{d}(\delta\boldsymbol{g}) = p_n\left[\delta\xi^i(\boldsymbol{n}\cdot\boldsymbol{t}_{i,j})\mathrm{d}\xi^j + \boldsymbol{n}\cdot(\mathrm{d}\boldsymbol{u}^t_{,i}\delta\xi^i + \delta\boldsymbol{u}^t_{,j}\mathrm{d}\xi^j)\right]. \tag{57}$$

The calculation of $\mathrm{d}(\delta\xi^j)$ is a little cumbersome, yet by taking the differentiation of Eq. (19), the final result can be found by solving the following equations:

$$\begin{aligned} A_{ij}\,\mathrm{d}(\delta\xi^j) = & -\boldsymbol{t}_i\cdot\delta\boldsymbol{u}^t_{,j}\mathrm{d}\xi^j - \boldsymbol{t}_i\cdot\mathrm{d}\boldsymbol{u}^t_{,j}\delta\xi^j - (\boldsymbol{t}_i\cdot\boldsymbol{t}_{j,l} + g\boldsymbol{n}\cdot\boldsymbol{t}_{i,jl})\delta\xi^j\mathrm{d}\xi^l \\ & - \delta\xi^j\boldsymbol{t}_j\cdot(\mathrm{d}\boldsymbol{u}^t_{,i} + \boldsymbol{t}_{i,l}\mathrm{d}\xi^l) - \mathrm{d}\xi^j\boldsymbol{t}_j\cdot(\delta\boldsymbol{u}^t_{,i} + \boldsymbol{t}_{i,l}\delta\xi^l) \\ & - (\boldsymbol{x}^t - \boldsymbol{x}^h)\cdot(\delta\boldsymbol{u}^t_{,ij}\mathrm{d}\xi^j + \mathrm{d}\boldsymbol{u}^t_{,ij}\delta\xi^j) \\ & - (\delta\boldsymbol{u}^t - \delta\boldsymbol{u}^h)\cdot(\mathrm{d}\boldsymbol{u}^t_{,i} + \boldsymbol{t}_{i,l}\mathrm{d}\xi^l) - (\mathrm{d}\boldsymbol{u}^t - \mathrm{d}\boldsymbol{u}^h)\cdot(\delta\boldsymbol{u}^t_{,i} + \boldsymbol{t}_{i,l}\delta\xi^l)\,, \end{aligned} \tag{58}$$

$$A_{ij} = (\boldsymbol{t}_i\cdot\boldsymbol{t}_j) + (\boldsymbol{x}^t - \boldsymbol{x}^h)\cdot\boldsymbol{t}_{i,j}\,. \tag{59}$$

It is seen that the tangent stiffness contributed by the kinematic action of contact point is symmetrical, due to the exchangeability between the differentiation and variation.

Next, based on the algorithm presented in Sec. 3.1, the differentiation of the friction force will be obtained by starting from the differentiation of Eqs. (47) and (52).

(1) Stick state:

Differentiation of Eq. (47) becomes

$$\begin{aligned} \mathrm{d}p_{tk(i+1)} = \varepsilon \Big[& \mathrm{d}(\boldsymbol{t}_k\cdot\boldsymbol{t}_j)_{(i+1)}({}^0\boldsymbol{t}^j_{(i+1)}\cdot\Delta^0\boldsymbol{r}) \\ & (\boldsymbol{t}_k\cdot\boldsymbol{t}_j)_{(i+1)}(\mathrm{d}^0\boldsymbol{t}^j_{(i+1)}\cdot\Delta^0\boldsymbol{r}) + (\boldsymbol{t}_k\cdot\boldsymbol{t}_j)_{(i+1)}({}^0\boldsymbol{t}^j_{(i+1)}\cdot\mathrm{d}\Delta^0\boldsymbol{r})\Big]\,. \end{aligned} \tag{60}$$

Applying

$$\mathrm{d}\boldsymbol{t}_{k(i+1)} = \boldsymbol{t}_{k(i+1),l}\mathrm{d}\xi^l + \mathrm{d}\boldsymbol{u}^t_{,k} \tag{61}$$

leads to

$$\mathrm{d}(\boldsymbol{t}_k \cdot \boldsymbol{t}_j)_{(i+1)} = (\boldsymbol{t}_{k(i+1),l} \cdot \boldsymbol{t}_{j(i+1)} + \boldsymbol{t}_{j(i+1),l} \cdot \boldsymbol{t}_{k(i+1)})\mathrm{d}\xi^l + \boldsymbol{t}_{k(i+1)} \cdot \mathrm{d}\boldsymbol{u}^t_{,j} + \boldsymbol{t}_{j(i+1)} \cdot \mathrm{d}\boldsymbol{u}^t_{,k} \,. \tag{62}$$

Use of the relationship between the covariant and contravariant base vectors at the mapped contact point in the reference configuration, namely,

$${}^0\boldsymbol{t}^j_{(i+1)} \cdot {}^0\boldsymbol{t}_{l(i+1)} = \delta^j_l \tag{63}$$

gives

$$\mathrm{d}^0\boldsymbol{t}^j_{(i+1)} \cdot {}^0\boldsymbol{t}_{l(i+1)} = -{}^0\boldsymbol{t}^j_{(i+1)} \cdot \mathrm{d}^0\boldsymbol{t}_{l(i+1)} \,. \tag{64}$$

By decomposing the mapping of the incremental relative displacement vector to be the form as

$$\Delta^0\boldsymbol{r} = \Delta^0 r^l \, {}^0\boldsymbol{t}_{l(i+1)} \tag{65}$$

and considering

$$\mathrm{d}^0\boldsymbol{t}_{l(i+1)} = {}^0\boldsymbol{t}_{l(i+1),m}\,\mathrm{d}\xi^m \tag{66}$$

and Eq. (64), it is given that

$$\mathrm{d}^0\boldsymbol{t}^j_{(i+1)} \cdot \Delta^0\boldsymbol{r} = -\Delta^0 r^l \, {}^0\boldsymbol{t}^j_{(i+1)} \cdot {}^0\boldsymbol{t}_{l(i+1),m}\,\mathrm{d}\xi^m \,. \tag{67}$$

On the other hand, by means of the definition of the covariant base vector at the mapped contact point in the reference configuration,

$$\mathrm{d}\Delta^0\boldsymbol{r} = {}^0\boldsymbol{t}_{l(i+1)}\,\mathrm{d}\xi^l \tag{68}$$

is obtained from Eq. (45). Then use of Eq. (63) yields

$${}^0\boldsymbol{t}^j_{(i+1)} \cdot \mathrm{d}\Delta^0\boldsymbol{r} = \mathrm{d}\xi^j \,. \tag{69}$$

Rearranging the above results, the differentiation of friction force is given as

$$\begin{aligned}\mathrm{d}p_{tk(i+1)} = \varepsilon \Big\{ \left({}^0\boldsymbol{t}^j_{(i+1)} \cdot \Delta^0\boldsymbol{r}\right) \Big[\left(\boldsymbol{t}_{k(i+1),l} \cdot \boldsymbol{t}_{j(i+1)} + \boldsymbol{t}_{j(i+1),l} \cdot \boldsymbol{t}_{k(i+1)}\right) \mathrm{d}\xi^l \\ + \boldsymbol{t}_{k(i+1)} \cdot \mathrm{d}\boldsymbol{u}^t_{,j} + \boldsymbol{t}_{j(i+1)} \cdot \mathrm{d}\boldsymbol{u}^t_{,k} \Big] \\ - (\boldsymbol{t}_k \cdot \boldsymbol{t}_j)_{(i+1)} \Delta^0 r^l \left({}^0\boldsymbol{t}^j_{(i+1)} \cdot {}^0\boldsymbol{t}_{l(i+1),m}\right) \mathrm{d}\xi^m + (\boldsymbol{t}_k \cdot \boldsymbol{t}_j)_{(i+1)}\,\mathrm{d}\xi^j \Big\} \,.\end{aligned} \tag{70}$$

(2) Slide state:

In this case, the differentiation of friction force can be derived from the differentiation of Eq. (52), namely,

$$\mathrm{d}p^{(F)}_{tk(i+1)} = \mu\,\mathrm{d}|\boldsymbol{p}_{n(i+1)}|T_{k(i+1)} + \mu|\boldsymbol{p}_{n(i+1)}|\mathrm{d}T_{k(i+1)} \,. \tag{71}$$

For $\mathrm{d}T_{k(i+1)}$, note that the covariant base vector is perpendicular to the contravariant one, Eq. (51) is differentiated to obtain

$$\mathrm{d}T_{k(i+1)} = \frac{\mathrm{d}p^{(T)}_{tk(i+1)}}{\left|\boldsymbol{p}^{(T)}_{t(i+1)}\right|} - \frac{\mathrm{d}p^{(T)}_{tj(i+1)}}{\left|\boldsymbol{p}^{(T)}_{t(i+1)}\right|} T_k T^j + T_k\, T^j\, \boldsymbol{T} \cdot \mathrm{d}\boldsymbol{t}_{j(i+1)} \tag{72}$$

where

$$T^j = \frac{p^{j(T)}_{t(i+1)}}{\left|\boldsymbol{p}^{(T)}_{t(i+1)}\right|} \tag{73}$$

represents the normalized trial friction force. Since $p_{n(i+1)} < 0$ in the contact state, the differentiation of friction force can be obtained in the following form:

$$\begin{aligned} \mathrm{d}p^{(F)}_{tk(i+1)} = &-\mu\,\mathrm{d}p_{n(i+1)}\,T_{k(i+1)} - \mu\,p_{n(i+1)}\,\frac{\mathrm{d}p^{(T)}_{tj(i+1)}}{\left|\boldsymbol{p}^{(T)}_{t(i+1)}\right|}(\delta^j_k - T_k T^j) \\ &- \mu\,p_{n(i+1)}\,T_k T^j\,\boldsymbol{T}\cdot\mathrm{d}\boldsymbol{t}_{j(i+1)}\,. \end{aligned} \tag{74}$$

It is observed from Eq. (70) or (74) that the tangent stiffness due to friction is nonsymmetrical. The general ***LDU*** decomposition method based on Gaussian elimination can be used to solve the nonsymmetric matrix equation. In this work, the skyline solver is used to take the advantage of saving memory space. However, since the active columns of both upper and lower triangular parts of stiffness matrix must be stored, the computation needs almost double as much memory space as the skyline algorithm applied to symmetric problems.

4. Numerical examples

Using the element local coordinates and their differentiations, the equivalent nodal contact force, friction force and tangent stiffness due to frictional contact can be constructed based on the formulation performed in Sec. 2. These are implemented into a finite element analysis code for large deformation elastoplastic problems developed by the authors. First, a two-leaf structure is analyzed to verify the effectiveness of the proposed algorithm. Then the analysis of a leaf spring structure used in nuclear power plants is carried out using a simplified model.

4.1. Frictional contact problem of a two-leaf structure

Figure 4 shows the geometry and the finite element mesh of a two-leaf structure. The depth of two leaves is set at 2 mm and the degrees of freedom in the out-of-plane direction are constrained. The left side of the upper leaf and the right side of the lower leaf are clamped to rigid walls. The leaves are then deformed by applying downward displacement on the left rigid wall. The penalty parameter used for the stick state is $\varepsilon = 1.0\mathrm{e}4$. In this example, the contact constraint is given such that the upper leaf cannot penetrate the lower one. Von Mises yield function and the associated flow rule with isotropic hardening are assumed for elastoplastic analysis. Also, the total Lagrangian formulation is adopted assuming small strain and large rotation [1]. The prescribed displacement $U = 30$ mm is equally divided into 60 steps, but as a result of computation, the two leaves separated before 30 mm was reached.

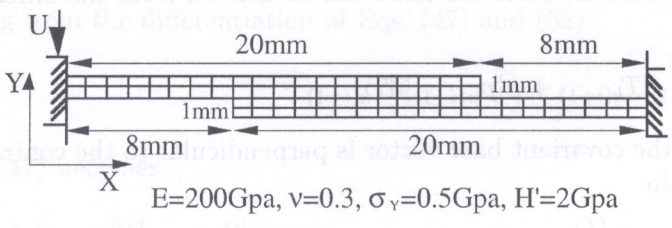

Fig. 4. Two-leaf frictional contact system

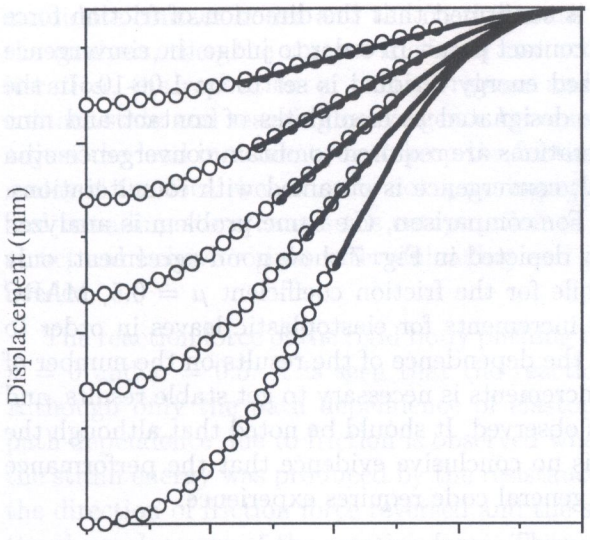

Fig. 5. Displacements of leaf surface

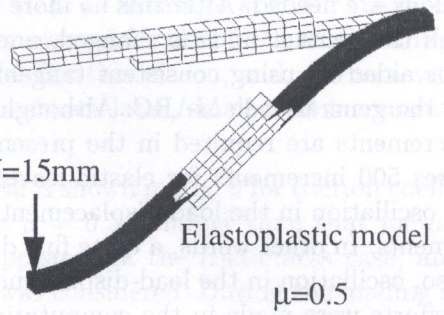

Fig. 6. Deformation of two leaves

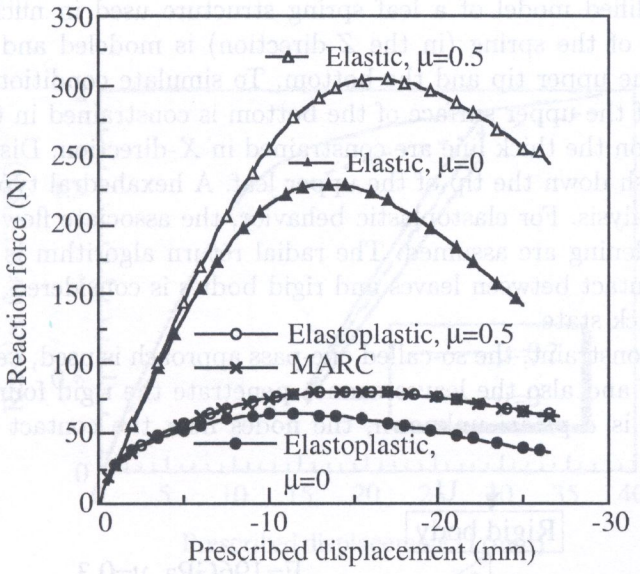

Fig. 7. Reaction force of rigid wall vs. prescribed displacement

The results for the coefficient of friction $\mu = 0.5$ are first shown. The nodal displacements on the contact surfaces of the upper and lower leaves are depicted in Fig. 5 for typical increments. Although it is illegible in the figure, the results show that the nodes on the free side released from the contact surface in early deformation due to the deflection of the leaf. Along with deformation, the contact nodes changed and the two leaves separated after the nodes of the free side made contact. Thus, the large amount of sliding of the contact node over the element boundary was successfully simulated. Figure 6 shows the deformation for the prescribed displacement, $U = 15$ mm, where the yielding area is shaded black.

The analysis of frictionless contact problems for elastic leaves is also performed for comparison. Figure 7 shows the relationship between the prescribed displacement and the reaction force of the rigid wall. As expected, the reaction force in the case of elastic leaves was larger than in the case of elastoplastic ones. Also, a larger reaction force due to friction was observed. In these analyses, smooth results were obtained despite the repetition of the contact and release of the contact nodes and sliding over the element boundary. Moreover, since the relative displacement at the contact point

is defined in the current deformed configuration, it is confirmed that the direction of friction force always coincides with the tangential direction at the contact point. In order to judge the convergence of iterative computation, tolerance for the normalized energy residual is set to be 1.0e-10. In the first load step, all nodes on the contact surface are designated as candidates of contact and nine iterations are needed. After this no more than six iterations are required to obtain convergence even though the contact node is changed, and in general, convergence is obtained with four iterations. This is aided by using consistent tangent stiffness. For comparison, the same problem is analyzed using the general code MARC. Although the results depicted in Fig. 7 show good agreement, only 60 increments are required in the present work, while for the friction coefficient $\mu = 0.5$, MARC requires 500 increments for elastic leaves and 1200 increments for elastoplastic leaves in order to avoid oscillation in the load-displacement curve and the dependence of the results on the number of increments. In other words, a quite fine division of increments is necessary to get stable results, and even so, oscillation in the load-displacement curve is observed. It should be noted that although the best efforts were made in the computations, there is no conclusive evidence that the performance has been perfectly executed, since treatment of the general code requires experience.

4.2. Frictional contact problem of a leaf spring structure

Figure 8 shows a simplified model of a leaf spring structure used in nuclear power plants. Due to symmetry, only half of the spring (in the Z-direction) is modeled and computed. Two leaves contact each other at the upper tip and the bottom. To simulate conditions under bolt fastening, the degree of freedom of the upper surface of the bottom is constrained in the Y-direction and the displacements of nodes on the thick line are constrained in X-direction. Displacement is prescribed to the rigid body to push down the tip of the upper leaf. A hexahedral type of element with eight nodes is used in the analysis. For elastoplastic behavior, the associate flow rule of von Mises type and isotropic work hardening are assumed. The radial return algorithm is adopted to update the stress. The frictional contact between leaves and rigid bodies is considered. Penalty parameter $\varepsilon =$ 1.0e5 is given for the stick state.

For the geometrical constraint, the so-called one-pass approach is used, i.e., the upper leaf cannot penetrate the lower leaf and also the leaves cannot penetrate the rigid foundation and rigid body. Since the contact state is *a priori* unknown, the nodes near the contact surface are selected as

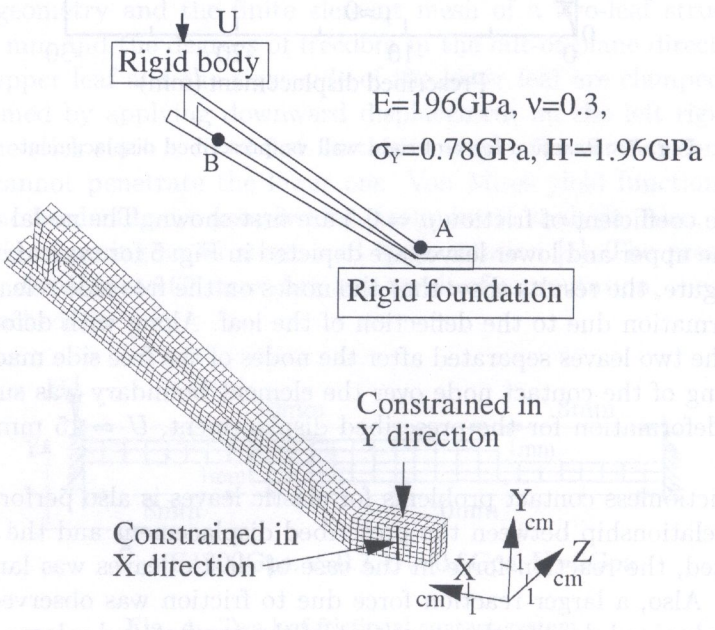

Fig. 8. Leaf spring loaded with prescribed displacement

candidate contact nodes and the friction state at all contact nodes is assumed to be stick to start the analysis, then the correct frictional contact state is found by a trial and error process. During iteration, the repetition of contact-release and stick-slide occurred due to the trial prediction of contact state and reaching convergence became difficult sometimes. In such a case, it is effective to adjust the load increment, or to keep the frictional contact state as release or stick for these contact nodes if the local behavior is not very important. The reverse of friction force at the unloading and reloading steps causes the computation to be unstable. For this reason, and also to reveal the structural behavior right after unloading and reloading as shown later, small load increments are needed.

The reaction force of the rigid body pushing the upper leaf is shown in Fig. 9 for friction coefficient $\mu = 0$ and $\mu = 0.5$. It is seen that the reaction force for $\mu = 0.5$ is larger than that for $\mu = 0$. Although only the path dependence of elastoplasticity appeared in the frictionless case, another path dependence due to friction is observed when friction was considered. During the loading stage, the strain energy was produced by the resistance of friction force. However, just after the unloading, the direction of friction force reversed and the strain energy was released suddenly. This resulted in the sharp decrease of the reaction force. Through the unloading process, the reaction force became lower than that for the frictionless case. On the other hand, in the reloading process, the situation became the inverse. The area enclosed by unloading and reloading process represents the energy dissipation due to friction.

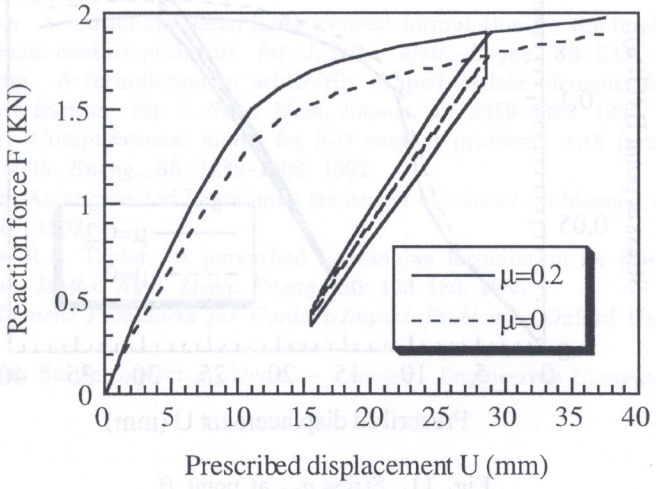

Fig. 9. Reaction force of rigid body vs. prescribed displacement

The maximum stress occurred at point A in Fig. 8, at the bottom of the upper leaf. The stress component σ_{xx} at point A and that at point B, the latter of which is near the contact area of the lower leaf as shown in Fig. 8, are shown in Figs. 10 and 11, respectively. Since point A is far from the contact area, the effect of friction on the stress was not clear. However at point B, the frictional contact relaxed the bending stress during the loading process. Therefore the stress in the friction case was lower than that in the frictionless one. Right after unloading, the friction state became stick and the friction force turned to the opposite direction. This resulted in the rapid recovery of the bending stress. Similarly, the stress at point B was affected by friction during the reloading process. From the above results it is realized that to get hold the structural responses of multi-leaf structures, the effect of frictional contact may be an important factor.

The deformation of the leaf spring with the largest prescribed displacement is shown in Fig. 12 and the yielding area is shaded black. Once the friction and contact states were determined, quadratic convergence was achieved by the use of consistent tangent stiffness.

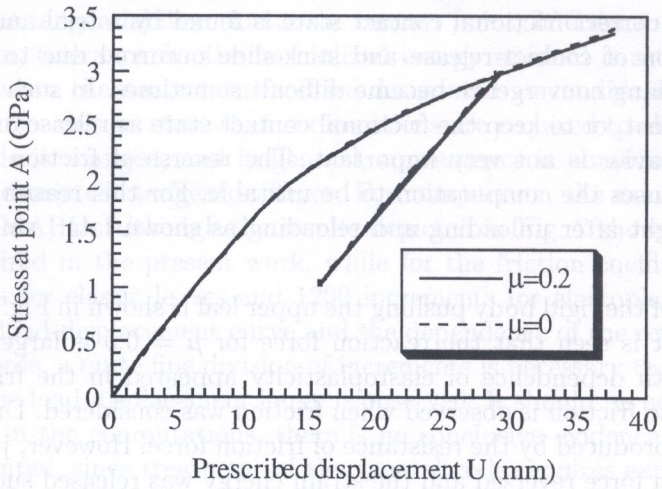

Fig. 10. Stress σ_{xx} at point A

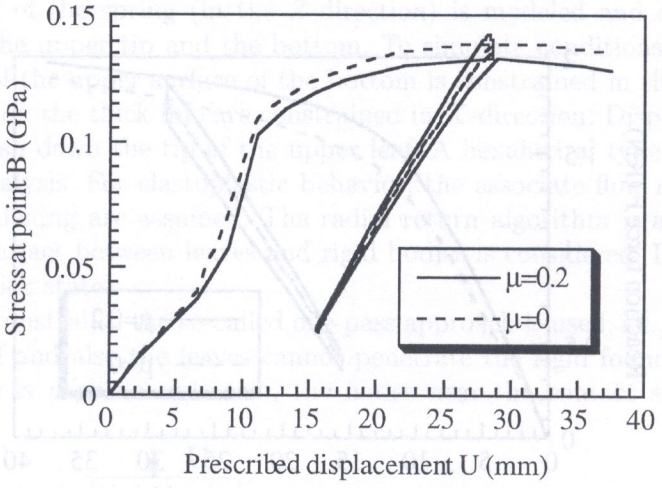

Fig. 11. Stress σ_{xx} at point B

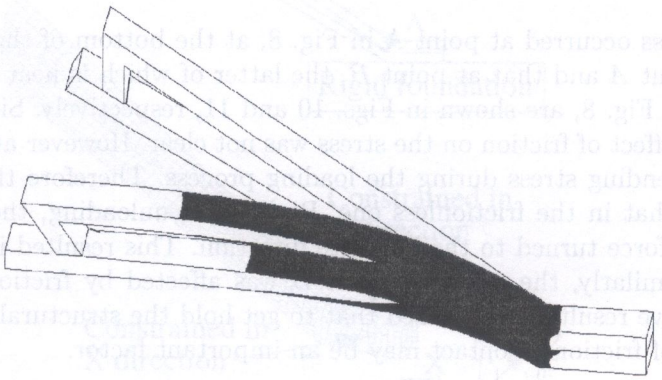

Fig. 12. Deformation of leaf spring

5. Conclusions

In this work, a finite element approach that enables the analysis of frictional contact problems including finite sliding was proposed for the design of multi-leaf structures. The method utilized the convected coordinate system so that the objectivity of the friction law was preserved. Conventional methods have not effectively dealt with the sliding that extends over the element boundary, whereas the proposed method solves this problem by redefining the slide term of friction law as a spatial vector in the reference configuration. In the formulation, the consistent tangent stiffness was derived to obtain quadratic convergence. The effectiveness of the proposed method was verified by numerical examples. The effect of frictional contact on the structural response of multi-leaf structures is revealed to cause another path dependence due to the friction besides the path dependence of elastoplasticity.

References

[1] K.-J. Bathe. *Finite Element Procedures.* Prentice Hall, 1996.

[2] R. Buczkowski, M. Kleiber. Elasto-plastic interface model for 3D-frictional orthotropic contact problems. *Int. J. Num. Meth. Engng.*, **40**: 599–619, 1997.

[3] T. Hisada. *Foundation of Tensor Analysis for Nonlinear Finite Element Method* (in Japanese). Maruzen, Tokyo, 1992.

[4] N. Kikuchi, J.T. Oden. Contact Problems in Elasticity: A Study of Variational Inequalities and Finite Element Methods. *SIAM*, Philadelphia, 1988.

[5] T.A. Laursen, J.C. Simo. A continuum-based finite element formulation for the implicit solution of multibody, large deformation frictional contact problems. *Int. J. Num. Meth. Engng.*, **36**: 3451–3485, 1993.

[6] H. Parisch, Ch. Lubbing. A formulation of arbitrarily shaped surface elements for three-dimensional large deformation contact with friction. *Int. J. Num. Meth. Engng.*, **40**: 3359–3383, 1997.

[7] D. Peric, D.R.J. Owen. Computational model for 3-D contact problems with friction based on the penalty method. *Int. J. Num. Meth. Engng.*, **35**: 1289–1309, 1992.

[8] J.C. Simo, T.A. Laursen. An augmented Lagrangian treatment of contact problems involving friction. *Computers & Structures*, **42**: 97–116, 1992.

[9] J.C. Simo, P. Wriggers, R.L. Taylor. A perturbed Lagrangian formulation for the finite element solution of contact problems. *Comp. Meths. Appl. Mech. Engng.*, **50**: 163–180, 1985.

[10] Z.-H. Zhong. *Finite Element Procedures for Contact-Impact Problems.* Oxford University Press, New York, 1993.

[11] Z.-H. Zhong, J. Mackerle. Static contact problems — a review. *Engineering Computations*, **9**: 3–37, 1992.